一般社団法人　電子情報通信学会
THE INSTITUTE OF ELECTRONICS,
INFORMATION AND COMMUNICATION ENGINEERS

信学技報
IEICE Technical Report
A・P2023-57(2023-07)

Qualification of ripple in medium Gain horns

Derek GRAY and Julien Le KERNEC

James Watt School of Engineering,　University of Glasgow,　Glasgow,　UK.

E-mail:　(Derek.Gray,　Julien.LeKernec) @glasgow.ac.uk

Abstract　A conventional rectangular mouth 25dBi pyramidal horn and an equivalent circular mouth spline horn were fully qualified by simulation in commercially available software across 54% relative bandwidth for sensing application in and around the ESA vacuum chamber at the University of Glasgow.　Both antenna types showed small-scale 0.2dB ripple in directivity, 3dB beamwidth and first sidelobe level caused by internal standing waves.　This represents about 0.5% of the power passing through the antennas.　Performance differences from feeding by either conventional rectangular waveguide proportions of 2:1 or 2:0.88 were investigated, as was the behaviour dependence of the waveguide to spline horn junction.

Keywords horn antenna,　directivity ripple.

1. Introduction

Horn antennas have been in widespread use for about 100 years [1].　The first successful E and H-plane pattern equalization to achieve a scalar feed was 80 years ago, demonstrating sophisticated control of the aperture distribution [2].　The received wisdom is that there must always be a compromise between Directivity and bandwidth.　An upper-medium directivity of 30dBi will come at the expense of narrow bandwidth.　The original interest in medium Gain horns was for lightweight switched beam antennas for the Japanese HAPS program to operate across all of Q-band.　Thus, the original aim was to civilianize prior airborne work such as the 1kg Multi-Platform Common Data Link (MP-CDL) antennas [3].　Other than the prohibitive computational burden of simulating medium Gain antennas across wideband, manually processing the excessive number of output data files was unfeasible.

Here that prior work is reappraised with relevance to Plume Surface Interaction (PSI) sensing applications in the ESA vacuum chamber at the University of Glasgow (UoG).　The aims were to develop a medium Gain horn at X-band that would be scaled to the as-yet-unknown target band and assess applicable means of high speed automated data processing to expedite the design process.

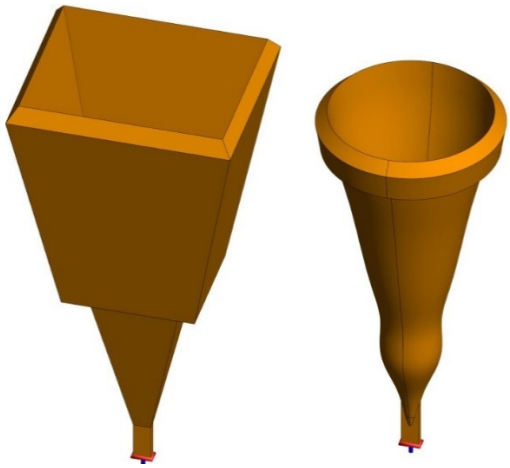

Figure 1:　CAD of pyramidal and spline horns;　to scale.

2. Model and process development

As noted in [4],　it is presumed that any antenna used within the vacuum chamber must be structurally robust enough to survive debris impact and be readily inspected and cleaned.　It is assumed that the antenna would be NC milled in-house at a low cost and conveniently repaired or replaced if seriously damaged.　Non-standard thick-walled horns are now commercially available from several manufacturers who make the CAD of their products freely available such as [5].　The rectangular

This article is a technical report without peer review, and its polished and/or extended version may be published elsewhere.
Copyright ©2023 by IEICE

pyramidal X-band horn used here had a length of 555mm, mouth dimensions of 267x217mm and wall thickness of 20mm, in contrast to the typical 5mm thickness [4]. This design thus has a pronounced bevel at the mouth edge, Figure 1. This was also used for the 430mm long near-conical spline horn. At 212mm diameter, the mouth of the spline horn fits entirely within the mouth of the rectangular pyramidal horn, thus being a shorter and credible lower-weight alternative design. Having high mass, neither would be suitable for use on a Moon or Mars soft lander.

Standard WR90 X-band rectangular waveguide has internal dimensions of 22.86x10.16mm, so having proportions of 2:0.88. The neighbouring WR62 has internal dimensions of 15.8x7.9mm, so having proportions of 2:1. Similarly, the majority of standard high *mm*-wave waveguides have 2:1 proportions, but some non-standard dimensioned transitions are commercially available. Consequently, the baseline pyramidal horn was simulated with WR90 and 22.86x11.43mm waveguide feed, labelled "pyramid WR90" and "pyramid 2:1" herein. The horn mouth and length were fixed giving a small difference in the E-plane flare angle. More attention was given to the latter due to the higher likelihood that it will be used as a scaled model. Conversely, a custom transition to coaxial cable or matching taper to the connection to the existing WR90 transitions will be needed for an X-band model.

The main aim of this work was to set up automated data post-processing for an example study of some wideband antenna simulated in a commercially available antenna simulator. Altair FEKO™ was chosen, as in common with its progenitor NEC, it produces text output files of primary and secondary computed quantities which are readily interrogated by a MATLAB™ code.

All the horns were simulated as "skin models" in FEKO™. These consisted of the inner surface of the horn, the mouth and as much of the outer wall surface as the MLFMM solver would tolerate, Figure 1. While the MLFMM solver gives a radical benefit in reducing computational burden, it tends to fail to converge for enclosed structures.

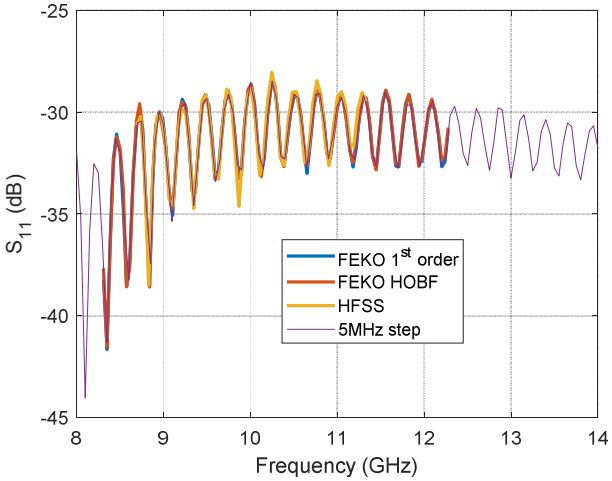

Figure 2: Simulated S_{11} of the "pyramid 2:1" horn.

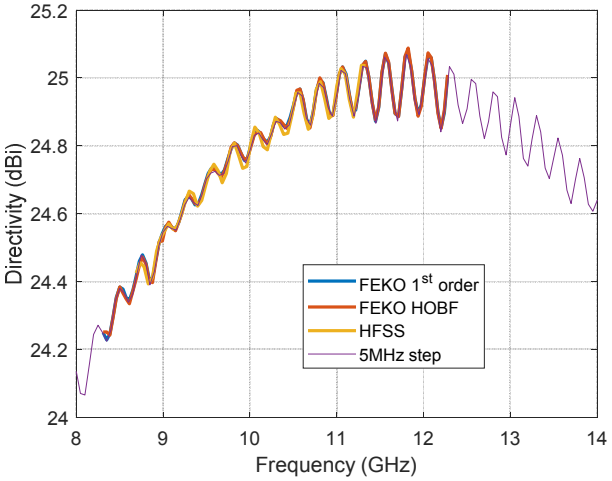

Figure 3: Simulated directivity of the "pyramid 2:1" horn.

The FEKO™ models in Figure 1 cannot be validated against measurement as no prototype antenna has been built yet. FEKO™ can discretize and solve a MOM model as 1st order basis function flat triangles or Higher Order Basis Function (HOBF) curvilinear elements which better represent curved structures. The pyramidal horn "pyramid 2:1" was simulated across 8.2 to 12.4GHz using both element types. It was also simulated in Ansys HFSS™, which due to the large electrical size of the horn necessitated implementation as a quarter model using both E and H-planes of symmetry. The near-perfect agreement was found between the 2 FEKO™ skin models and the HFSS™ quarter model for both S_{11} and peak

directivity, Figures 2 and 3. The FEKO™ model was redrawn with improved parametric control, and the trial and error process to find the longest outer wall length acceptable to the MLFMM solver for the extended 8 to 14GHz bandwidth was labelled "5MHz" here. Across 8.2 to 12.4GHz there was excellent agreement with the previous modelling, Figures 2 and 3.

Having validated the "pyramid 2:1" skin model, the choice of 5MHz frequency step had to be assessed to see if it was a sufficiently fine sampling of the frequency-dependent directivity oscillations. The peaks and troughs in the "5MHz" Directivity data from Figure 3 were located automatically and the relative difference between each neighbouring peak and trough pair was calculated. This directivity differential ranged from 0 to 0.2dB across 8 to 14GHz while the frequency step ranged from 80 to 200MHz, Figures 4 and 5. This horn had a 0.2dB ripple in its Directivity across 54% bandwidth. Between 11 and 12GHz the Directivity differential was relatively constant, ranging from 0.12 to 0.2dB, while the frequency step was constant at 120MHz; this band was chosen for evaluating the 5MHz frequency step data. The FEKO™ model was rerun from 11 to 12GHz with a 1MHz frequency step, Figure 6. Most of the "5MHz" troughs aligned with the 1MHz data, but most of the peaks did not, so the neighbouring peak-trough Directivity differential range was truncated, Figure 7. However a B-spline fit through the 5MHz data near perfectly matched the 1MHz data, Figure 6. The differential of the raw 5MHz and B-spline fit were compared, and it was found that the B-spline fit was less truncated above 10.5GHz by 0.015dB. Thus lower computational burden 5MHz frequency step was acceptable with B-spline fit prior to data metric extraction.

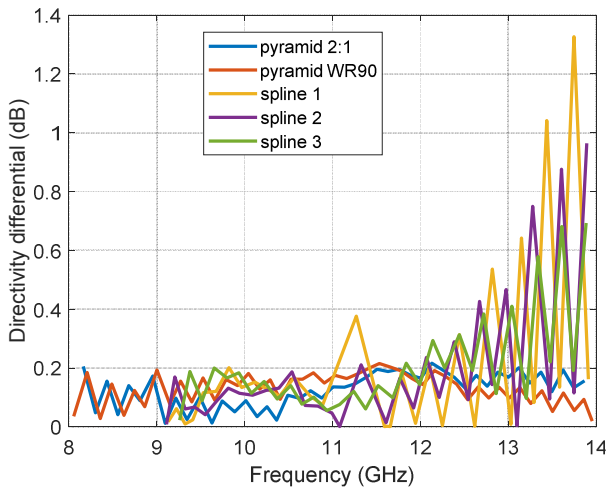

Figure 4: Directivity differences of neighbouring peak-trough pairs; from Figure 3 "5MHz" data.

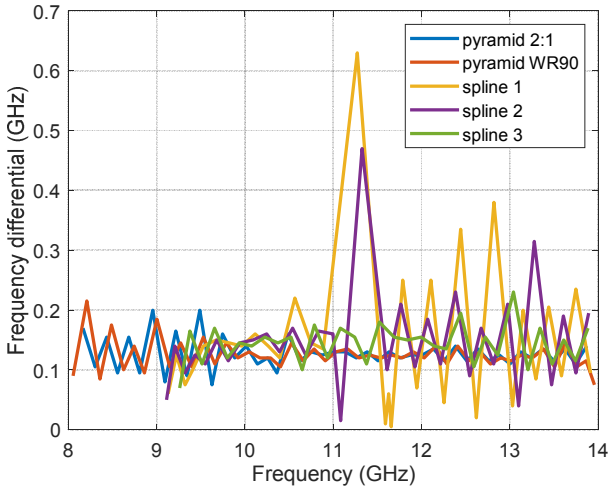

Figure 5: Frequency differences of neighbouring peak-trough pairs; from Figure 3 "5MHz" data.

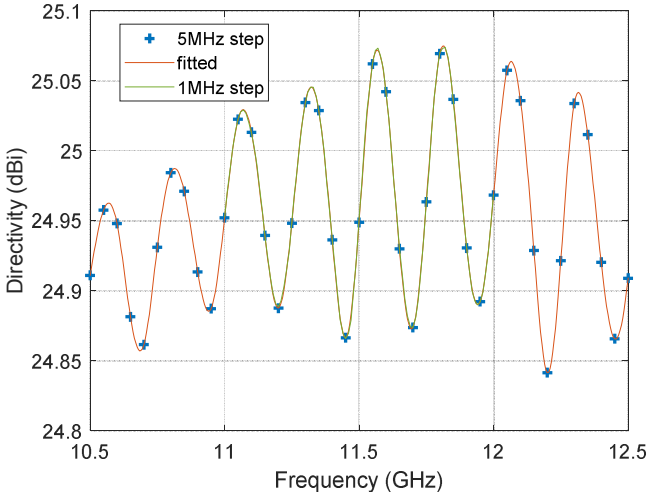

Figure 6: Effect of frequency step on the resolution of directivity ripple of "pyramid 2:1" horn.

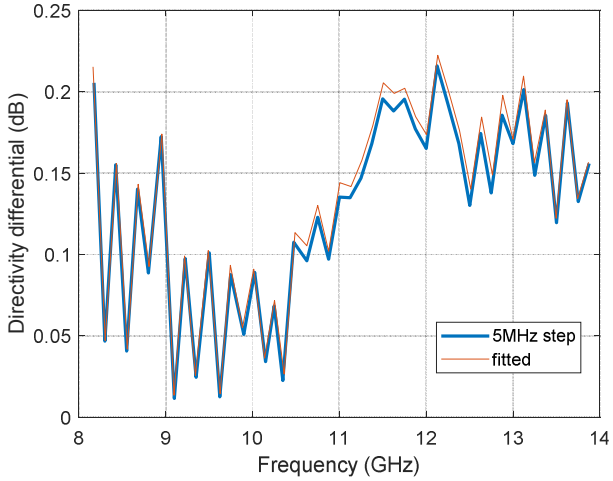

Figure 7: Effect of truncation on the range of directivity differences between neighbouring peak-trough pairs.

The ripple in the S_{11} was expected while that in the peak Directivity was not. The primary radiation mechanism is understood to be a Transverse Magnetic leaky wave on the inside of the E-plane walls of the pyramidal horn. The currents on the centre line of those walls were extracted at the peak and trough frequencies from the 1MHz dataset shown in Figure 6.

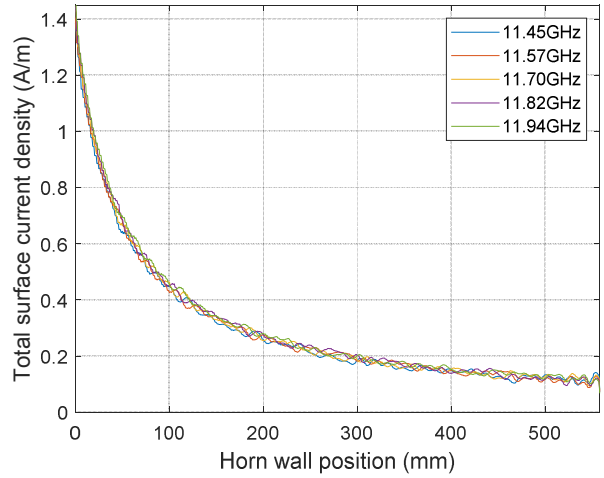

Figure 8: Simulated total surface current density along the centre line of an E-plane flare wall of "pyramid 2:1".

There was no apparent pattern in the magnitude of the total surface current density through the trough-peak-trough-… sequence, Figure 8. All 5 characteristics followed the same exponential decay as expected from decreasing current density with the spread of the surface area of the horn wall flare and power radiating off the surface. The real component of the same data did show a pattern in that for troughs the amplitude was high and for peaks low, Figure 9. Superficially, the phase relationship between the TM leaky wave on the horn E-plane walls and the radiated signal in the air guided by the horn caused the Directivity oscillations.

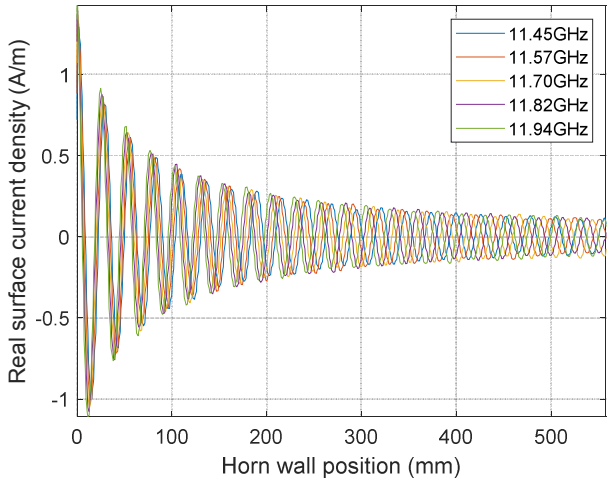

Figure 9: Real component of simulated total surface current density along the centre line of an E-plane flare wall of "pyramid 2:1".

The principal plane radiation patterns were as expected in that the E-plane pattern had high sidelobes from a poor aperture distribution while there was a quasi-Gaussian pattern in the H-plane, Figure 10.

The ripple was in all of the standard metrics, Figures 11 to 14. The E-plane 3dB beamwidth ranged from 9.5° to 7.5° and back to 9.5°, Figure 11. The H-plane 3dB beamwidth likewise ranged across 11° to 9.5°, having about 0.5° ripple above 11GHz, Figure 12. Similarly, the ripple in the first sidelobe level was greater in the H-plane than in the E-plane, Figures 13 and 14.

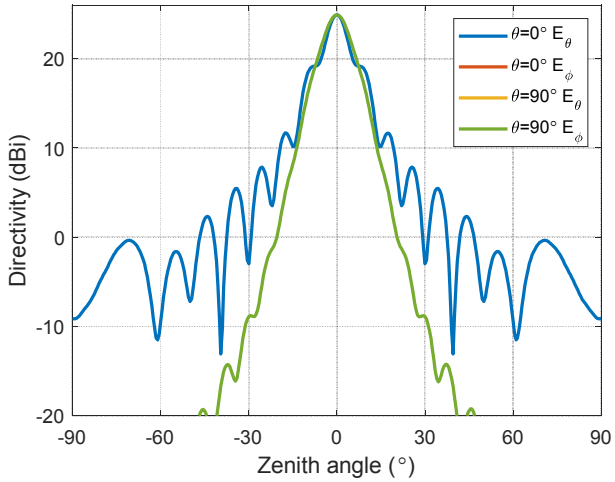

Figure 10: Simulated 11GHz radiation patterns of pyramidal horn "pyramid 2:1".

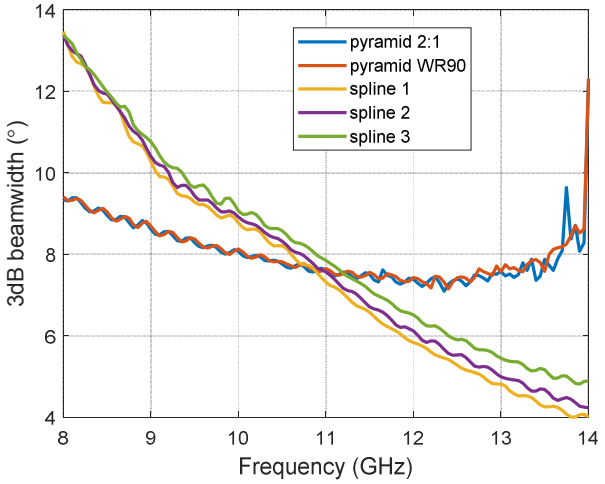

Figure 11: Simulated E-plane 3dB beamwidth.

3. Pyramidal horn study

The good agreement between the simple FEKO™ skin models meshed as first-order flat triangles to HOBF curvilinear meshed and the Finite Element Method HFSS™ showed the soundness of that model so confident to use that model type for a wideband horn study.

Reducing the rectangular guide height from 11.43mm to 10.16mm to form standard WR90 caused a small increase in the S_{11}, Figure 15. The Directivity ripple between 9 and 11.5GHz increased but the peak-trough spacing was unchanged indicating that the resonant effect was constant, Figures 4, 5 and 16. There were some minor changes in the E-plane 3dB beamwidth and 1st sidelobe levels, and none in the H-plane, indicating that the 2 horns were close to identical, Figures 11 to 14.

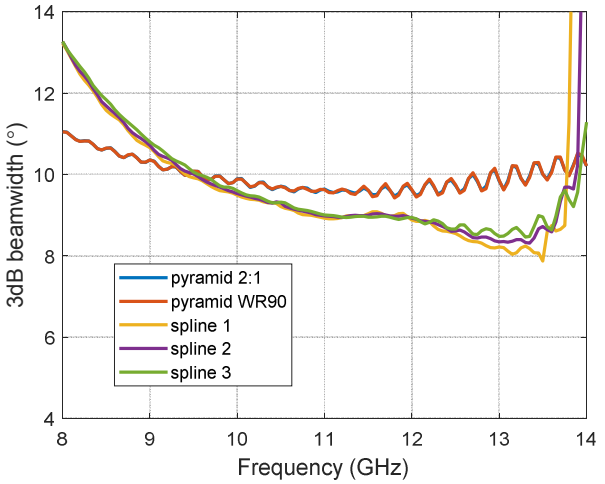

Figure 12: Simulated H-plane 3dB beamwidth.

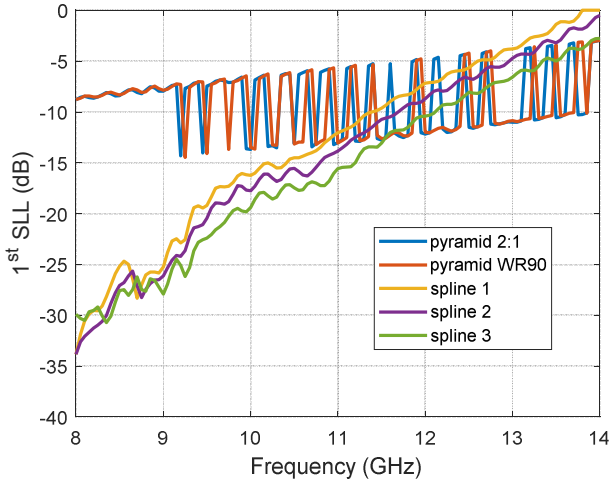

Figure 13: Simulated E-plane 1st sidelobe level variation across X-band.

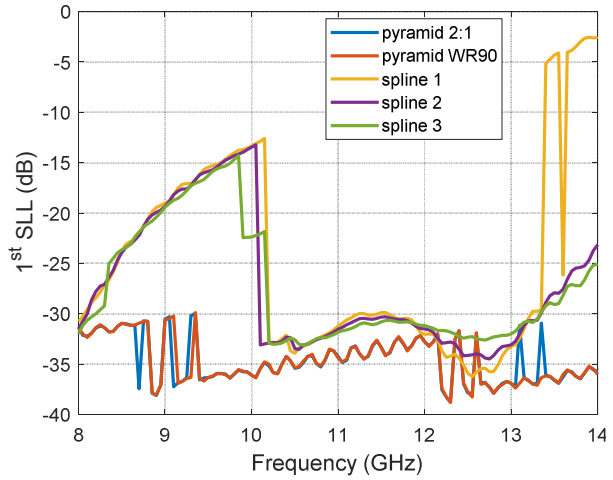

Figure 14: Simulated H-plane 1st sidelobe level variation across the band.

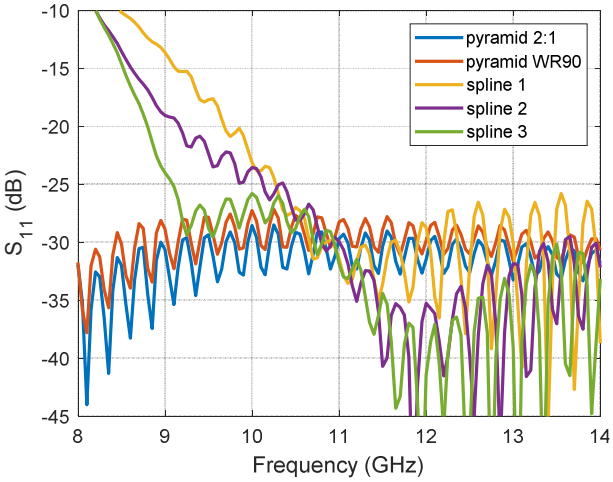

Figure 15: Simulated S_{11} of horns.

4. Spline horn study

The spline horn with WR90 feed from [4] based on [6] was redrawn in FEKO™ and the trial and error process to find an outer skin length for which the MLFMM solver

converged was undertaken, Figure 1. The only change trialled was stretching the taper below 150mm in steps to become close to a straight cone. As this lower section became a less abrupt transition from the waveguide to the almost constant radius section between 150 and 180mm as shown in Figure 17, the low-frequency S_{11} improved to have $S_{11} \leq$-10dB across all of the X-band and the E-plane 1st sidelobe level decreased, Figures 13 and 15. The latter indicated an improved aperture distribution which gave higher Directivity / efficiency above 9.5GHz, Figures 16 and 18. The radiation pattern was cleaner , Figure 19.

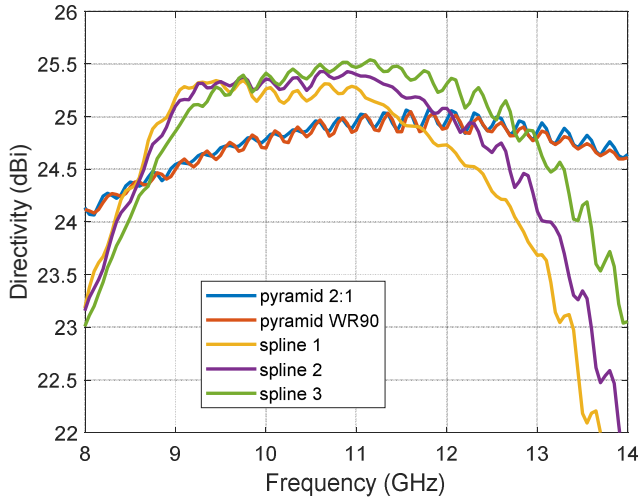

Figure 16: Simulated Directivity of horns.

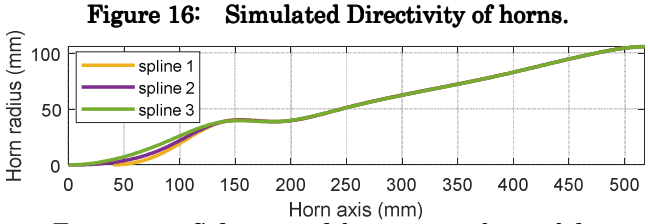

Figure 17: Splines used for inner surfaces of the rotationally symmetric spline horns.

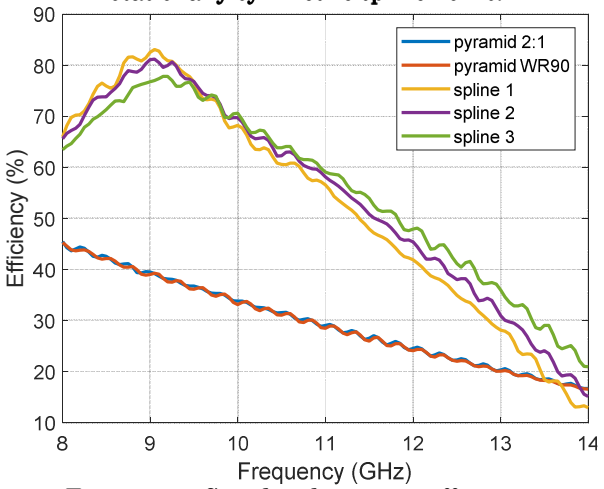

Figure 18: Simulated aperture efficiency.

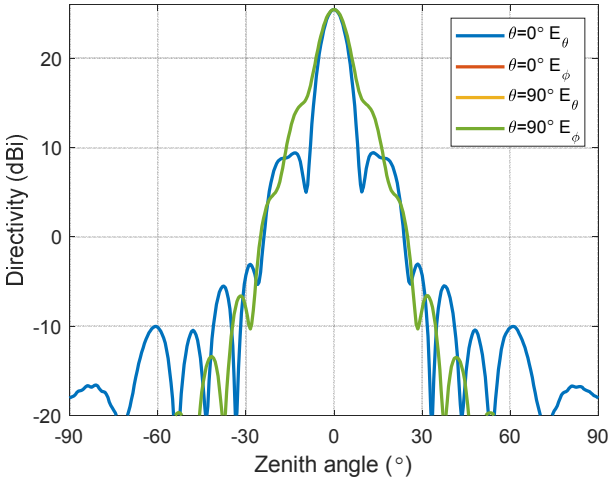

Figure 19: Simulated 11GHz radiation patterns of "spline3"; from FEKO™.

5. Conclusions and future work

A Matlab™ code to rapidly and accurately extract standard metrics from 100s to 1000s of antenna simulator output files was developed and demonstrated. Medium Gain horn antennas were used as the test case. Both the rectangular pyramidal and circular mouth spline horns were found to suffer 0.2dB directivity ripple which may affect wideband sensing applications. It was observed that spline horn transition performance is sensitive to the waveguide feed transition. Wideband horns will be designed for sensing applications in the vacuum chamber at UoG when the band and specifications are set.

Acknowledgement

The primary author is indebted to Dr C. Granet for the spline horn tutorial in Innis & Gunn during EUCap 2007.

8. References

[1] G.C. Southworth, "Short wave radio system," *United States patent 2,206,923*, granted July 9th, 1940.

[2] M. Katzin, "Electromagnetic wave horn radiator," *United States patent 2,317,464* granted April 27th, 1943.

[3] W. Williams & C. Burton, "Lightweight agile beam antennas for UAVS," *IEEE Military Communications conf. MILCOM*, 2006.

[4] D. Gray, J. Le Kernec & K. Kontis, "Integrated transition with dielectric rod for vacuum chamber," *IEICE Tech. Rep.*, Hiroshima Institute of Technology, vol. 122, no. 339, AP2022-179, pp. 12-17, Jan. 2023.

[5] www.eravant.com, accessed 17th of June, 2023.

[6] C. Granet, G.L. James, R. Bolton & G. Moorey, "A smooth-walled spline-profile hom as an alternative to the corrugated horn for wide band millimeter-wave applications," *IEEE Trans Antennas Propag.*, Vol. 52, No 3, March 2004, pp. 848-854.